Proceedings of ISFOG 2025
5TH INTERNATIONAL SYMPOSIUM ON
FRONTIERS IN OFFSHORE GEOTECHNICS
Nantes, France | June 9-13 2025

ISBN 978-2-85782-758-0

Geotechnical Analysis and Modeling for Offshore Wind Turbine Monopiles in Gulf of Bothnia Soil Conditions

M. Rova*
Geobotnia Oy, Oulu, Finland

A. Tuomela, A.H. Niemi
Civil Engineering Research Unit, University of Oulu, Oulu, Finland

J. Herva
Geobotnia Oy, Oulu, Finland

**milja.rova@geobotnia.fi*

ABSTRACT: Offshore wind energy is currently experiencing a period of rapid growth both globally and in Finland. Over the past decade, wind turbines have been installed in the sea areas of Northern Finland, and the size of wind farms has also increased. There are numerous methods for installing wind turbines, but the most common offshore wind farm foundation in Europe is the monopile. This paper analyses the modeling of sandy soil behavior under complex cyclic wind and ice loads. The advanced soil models SANISAND-MS and Hardening soil small (HSsmall) are used. The loads were simulated using the ice load portal developed by the Technical Research Centre of Finland (VTT). Modeling was carried out using Plaxis 3D with a 15MW virtual wind turbine with a 10-meter diameter monopile foundation published by the National Renewable Energy Laboratory (NREL). The study examines the soil deformation induced by both cyclic and static loading, as well as the displacement of the monopile foundation in various loading conditions. The results showed that under cyclic loading, the displacements increased after each load cycle, creating permanent soil deformations. For low design loads, the magnitudes of displacement predicted by SANISAND-MS and HSsmall were found to be of the same magnitude. However, differences between the material models were observed as the load magnitudes increased. The HSsmall model showed larger displacements in dynamic analyses compared to similar static loading scenarios. The SANISAND-MS model encountered numerical problems and failed to simulate the monopile foundation under storm loading conditions.

Keywords: Cyclic loading; Monopile foundation; 3D modeling

1 INTRODUCTION

The construction of wind turbines in Finland's northern conditions in sea areas has become more common in the last decade. The main challenges are a consequence of the extreme environmental conditions, which result in cyclical loads for the foundations of offshore wind turbines (Meng et al. 2024). The size of power plants has been constantly increasing, and even larger power plants will be constructed at greater distances from the mainland in the future. The mean size of wind farms built between 2016 and 2022 has doubled (Ramirez 2023). Offshore wind turbines are being installed in deeper waters, which further increases the size of the required foundation and brings challenges to the design of power plants and their foundations.

A monopile foundation represents a possible solution for the construction of offshore wind turbines situated at greater distances from the mainland. The monopile, which is a hollow steel pile typically with a diameter of between 4–12 m which is submerged into the seabed at depths between 20–40 m, with the water depth between 30–50 m (Wu et al. 2019).

This paper analyses the 3D modeling of sandy soil behavior under complex cyclic wind and ice loads. This paper presents a comparative analysis of the advanced soil models SANISAND-MS and Hardening Soil Small (HSsmall). The modeled wind turbine has a monopile foundation with a 10-meter outer diameter. The study investigates the soil deformations caused by cyclic and static loads, as well as the displacement of the monopile foundation under various load conditions. These loads have been simulated using the ice load portal, which was developed by the Technical Research Centre of Finland (VTT). The FE simulation is conducted using Plaxis 3D software.

2 DATA AND METHOD

2.1 Wind turbine properties

The modeled wind turbine is based on the National Renewable Energy Laboratory 15MW virtual wind turbine model. The hub height of a wind turbine is 150 m, the rotor radius is 120 m, and the water depth is 30 m (Gaertner et al. 2020).

2.2 Monopile model structure

A monopile is a steel hollow pile that has been modeled with plate elements with a modulus of elasticity E=210 GPa and a Poisson ratio of ν = 0.3. The pile has a length of 60 m, and a wall thickness of 140 mm. A beam is modeled on the neutral axis of the pile, with a modulus of elasticity that is a thousandth of that of the plate element. Consequently, the beam can be assumed to have no significant effect on the monopile foundation. The purpose of the beam element is to facilitate the analysis of pile displacement.

Additionally, a rigid plate element is modeled at the head of the pile, exhibiting a modulus of elasticity that is one thousand times greater than that of the pile's plate element. The plate element is added to reduce large unreal deformations at the head of the pile due to point load. The modeled monopile is illustrated in Figure 1. (Rova 2024)

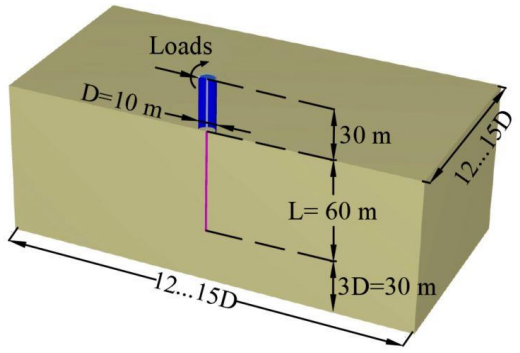

Figure 1. The model in Plaxis 3D (Rova 2024).

2.3 Soil model

The soil parameters of sand have been sourced from existing literature, but they align with the typical soil conditions observed in the Gulf of Bothnia (Rova 2024).

For loose sand, the unit weight is 16.5 kN/m^3 and the effective unit weight is 13.9 kN/m^3 (Liu et. al 2022). The friction angle of sand φ is 32° and the dilation angle ψ is 2° (Bentley 2023a). Pile installation effects are ignored and for installation the Mohr-Coulomb material model is used and for which Young's modulus E_{ref} is 20000 kN/m^2 (Rova 2024).

The parameters of the SANISAND-MS and the HSsmall material model for loose sand are presented in Table 1. and 2. SANISAND-MS is a bounding surface model which is developed to model cyclic deformation in sandy soils. The material model can account for changes in soil strength and soil stress over multiple loading cycles under drained state (Bentley 2023a). For a more detailed discussion of the material model parameters symbols, please refer to Liu et al. (2020) and Bentley (2023b).

Table 1. SANISAND-MS parameters (Liu et al. 2020).

Symbol	Parameter
G_0	95
ν	0,05
M_c	1,35
c	0,81
λ	0,055
e_c	1,035
ξ	0,36
m	0,01
h_0	7,6
c_h	0,97
n_b	1,2
A_0	0,74
n_d	1,79
μ_0	200
ζ	0,0005
β	4

Table 2. HSsmall parameters (Bentley 2023b).

Symbol	Parameter
E_{50ref}	20000 MPa
E_{oedref}	60000 MPa
$E_{ur\ ref}$	16000 MPa
G_{0ref}	70000 MPa
γ0,7	0,0001
ν	0,2
m	0,65

2.4 Cyclic loads

The design loads have been simulated in accordance with the specified wind turbine location. Cyclic ice loads have been simulated in VTT's ice load portal according to the design standard IEC-61400-3 (VTT 2024). An ice cone model developed by VTT was used to simulate the ice load, with ice thickness of 90 cm. The ice load portal was used to simulate a 600 s ice load, and the simulated ice load function is presented in Figure 2. The ice load function

demonstrates a situation where ice strikes the foundation and causes cyclic load peaks.

A 1-hour cyclic load modelling was performed in Plaxis 3D calculation software, for which the 600 s ice load function was generated from six consecutive 600 s simulated load functions. In Plaxis 3D, the cyclic load is added as a dynamic multiplier. (Rova 2024)

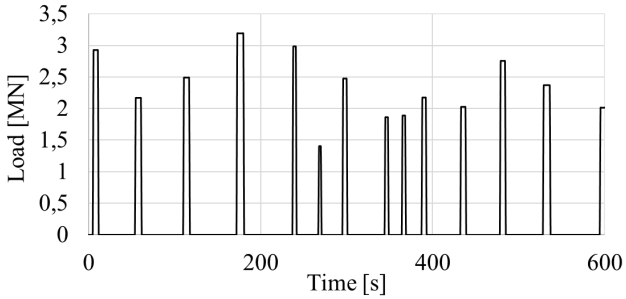

Figure 2. 600 s ice load simulated in the ice load portal (VTT 2024).

The wind load has been simulated in the ice load portal according to IEC 61400-1 turbulent wind model (VTT 2024). The wind also causes a moment, and it is represented as a wind moment load at the mudline. For simplification and enhanced convergence, the wind load and wind moment load have been modeled as static loads in Plaxis 3D. The magnitude of the static wind load is calculated from the cyclic simulated wind load and converted to static load by taking the average from the cyclic wind load. Additionally, the wind load has been calculated according to a theoretical formula presented by Arany et al. (2017), to achieve a smaller magnitude wind load. In this case, the wind turbine's nominal wind speed of 36 km/h is used.

The analyzed load scenarios are outlined in Table 3 where loads are multiplied by a factor of safety that is set at 1,35. The simulated storm wind load is 9342 kN and normal wind scenario wind load is 1494 kN. The loads are concentrated at the head of the pile as a point load, and furthermore, each calculation considers the dead weight of the wind turbine as a line load of 921 kN/m (Rova 2024).

Table 3. Modeled load scenarios (Rova 2024).

Model	Ice load [kN]	Wind load [kN]	Wind moment load [MNm]	Calculation type
1*	Cyclic	1494	224	Dynamic
2**	Cyclic	1494	224	Dynamic
3**	Cyclic	9342	1401	Dynamic
4**	Cyclic	Cyclic	1401	Dynamic
5*	Cyclic	1494	224	Dynamic
6*	2156	1494	224	Elasto-plastic
7**	2156	1494	224	Elasto-plastic
8*	2156	9340	1401	Elasto-plastic
9**	2156	9340	1401	Elasto-plastic

*SANISAND-MS material model
**HSsmall material model

3 RESULTS

3.1 Monopile displacement

Figure 3 illustrates the displacement of the monopile foundation, displaying the horizontal displacement of the pile for models 1, 2, 6 and 7 as a function of depth. The SANISAND-MS material model indicates that pile displacement on the mudline under cyclic loading conditions is approximately 60 mm, while the HSsmall material model and static load conditions suggest a pile displacement of approximately 30 mm (Rova 2024).

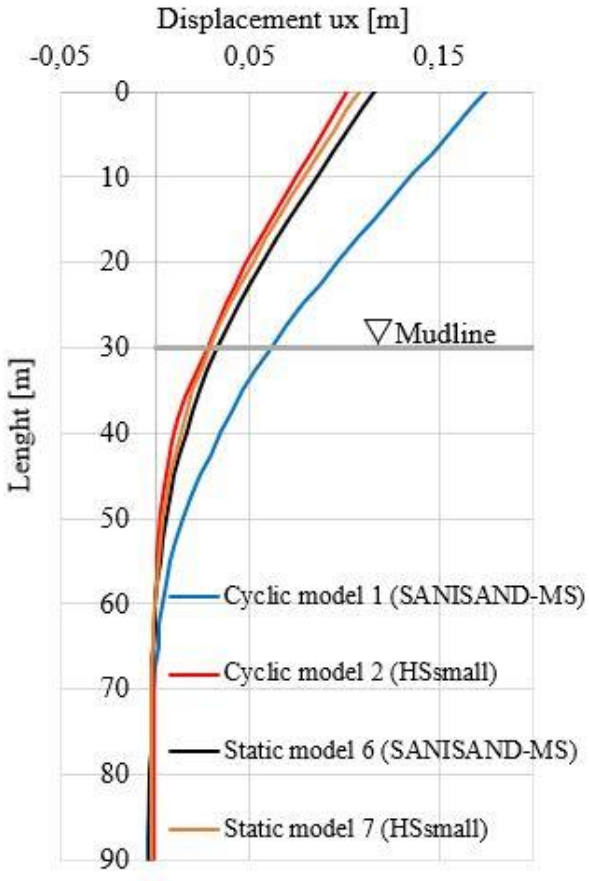

Figure 3. Monopile displacement during cyclic loading (Model 1 and 2) and displacement during static loading (Model 6 and 7) (Rova 2024).

As the loads increase, the magnitude of the displacement also increases, as illustrated in Figure 4. The displacement caused by static and cyclic wind loads and cyclic ice loads on the mudline in models 3 and 4 is of the same magnitude, reaching 480–540 mm. In a comparable, static load scenario in models 8 and 9, the pile displacement on the mudline was observed to be 210–270 mm. (Rova 2024)

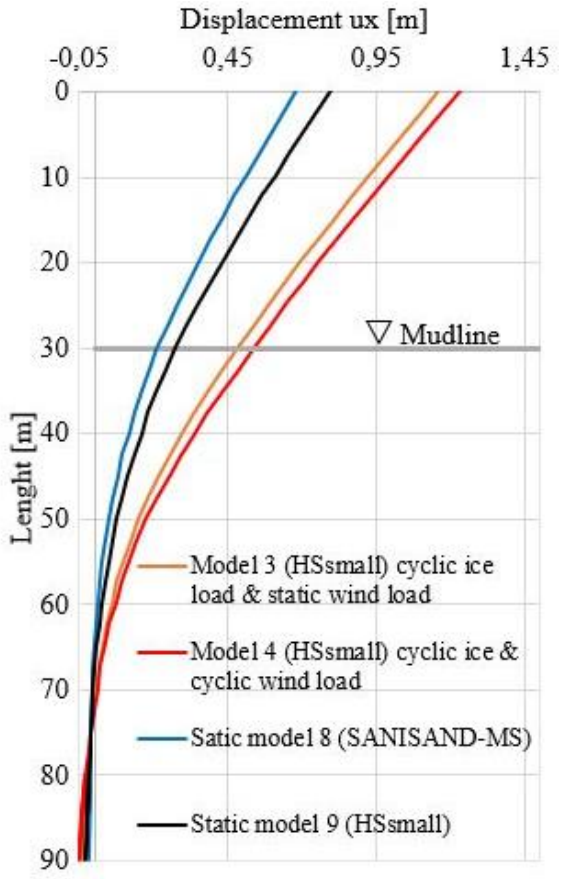

Figure 4. Monopile displacement when monopile is loaded with cyclic ice load and static wind load (Model 3), when both ice and wind loads are cyclic (Model 4) and when the loads are static (Model 8 and 9) (Rova 2024).

The displacement of the monopile foundation has been examined in Model 5 under a loading-unloading scenario. Figure 5 illustrates the displacement of the pile on the seabed as a function of time. During the application of cyclic loading, the pile displacement increases with each subsequent load cycle. However, between the unloaded phases, the displacement does not return to zero, resulting in the development of permanent displacements. The magnitude of the permanent displacement between unloaded phases is 10–15 mm. The total magnitude of the permanent displacement is approximately 35 mm in comparison to the initial state. (Rova 2024)

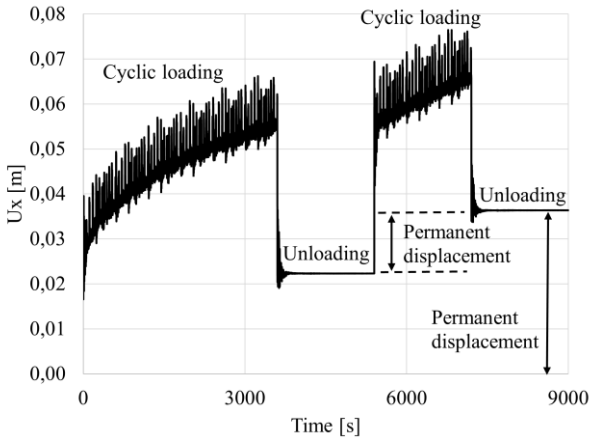

Figure 5. Model 5 (SANISAND-MS) monopile displacement on the mudline during loading-unloading (Rova 2024).

To solve the rotation of the pile on the seabed, two calculation points of the plate element have been selected. The points are situated on the mudline. Table 4 presents the total rotation values for different load scenarios. In the case of Model 5, the magnitude of the rotation has not been considered. The rotations have been calculated using a formula obtained from the literature (Bentley 2023a). In dynamic models, the total rotation is calculated following an hour-long cyclic load, with variations in rotation magnitude between cycles not considered. According to DNV-ST-0126 (2021), the rotation of the monopile foundation should not exceed 0.5°. In model 4, the rotation limit is exceeded; however, in the other modelling scenarios, the rotation magnitude is below the limit value. A distinguishing feature of Model 4 is its representation of both the ice and wind loads as cyclic loads, a distinction that is likely to yield a higher rotation value in comparison to the other modelling scenarios. (Rova 2024)

Table 4. Modeled load scenarios (Rova 2024).

Model name and material model	Rotation [°]
Cyclic model 1 (SANISAND-MS)	0,08
Cyclic model 2 (HSsmall)	0,05
Cyclic model 3 (HSsmall)	0,50
Cyclic model 4 (HSsmall)	0,52
Static model 6 (SANISAND-MS)	0,06
Static model 7 (HSsmall)	0,05
Static model 8 (SANISAND-MS)	0,32
Static model 9 (HSsmall)	0,36

3.2 Soil deformation

The modeling results show that permanent deformations have occurred in the soil for each

loading scenario. The value of permanent deformations is found to correlate with both the magnitude of the load applied and the duration of the loading period. Soil deformation is expressed as soil displacement and Table 5 shows the maximum soil displacement at the end of the modeling under different loading conditions. (Rova 2024)

Table 5. Maximum soil displacement under different load conditions at the end of modeling (Rova 2024).

Model and material model	Soil displacement
Cyclic model 1 (SANISAND-MS)	0,575 m
Cyclic model 2 (HSsmall)	0,042 m
Cyclic model 3 (HSsmall)	0,588 m
Cyclic model 4 (HSsmall)	0,651 m
Static model 6 (SANISAND-MS)	0,037 m
Static model 7 (HSsmall)	0,033 m
Static model 8 (SANISAND-MS)	0,236 m
Static model 9 (HSsmall)	0,301 m

One cause of soil deformation is an increase in pore pressure due to loading. In Plaxis 3D software, positive pore water pressure in the soil represents suction and negative pore water pressure represents compression (Bentley 2023b). This means that negative pore water pressure reduces the effective stress and, conversely, positive pore water pressure increases the effective stress, which increases soil strength. (Rova 2024)

Four calculation points were chosen to investigate pore water pressure, where (x, y, z) are A (7, 0, -50), B (15, 0, -50), C (7, 0, -80) and D (15, 0, -80). From the pore water pressure graph in Figure 6, it can be observed that the pore water overpressure increases or decreases when the ice load peak is activated, i.e. the pore water overpressure follows the amplitude of the cyclic ice load. (Rova 2024)

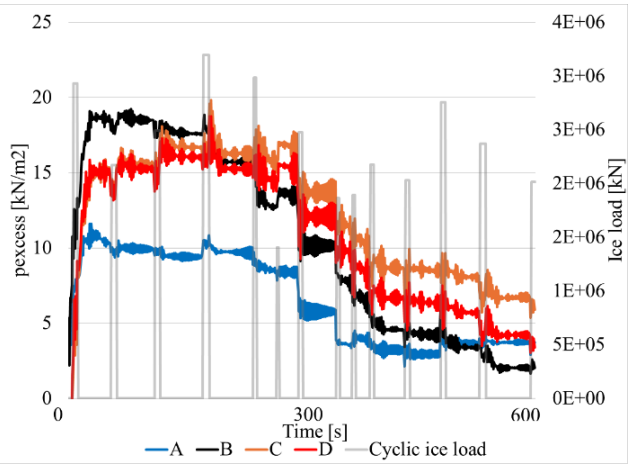

Figure 6. Pore water pressure during cyclic loading model 1 (SANISAND-MS) (Rova 2024).

The pore water pressure increases under cyclic loading, but in cyclic model 1 (SANISAND-MS) and cyclic model 2 (HSsmall), the excess pore water pressure does not increase significantly. However, an increase in pore water pressure causes deformation in the soil, and in the case of model 1 (SANISAND-MS), plastic points occur around the pile and on the soil surface as shown in Figure 7. (Rova 2024)

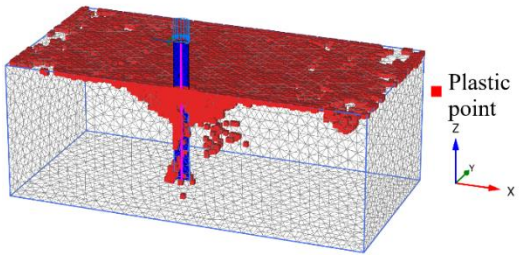

Figure 7. Plastic points during cyclic loading model 1 (SANISAND-MS) (Rova 2024).

When modeling with the HSsmall material model (2–4), a decrease in soil strength can be seen visually. Figure 8 shows that the weakened zone (blue) of model 2 (HSsmall) not only surrounds the pile but also expands under the influence of cyclic loading as illustrated in Figure 9. (Rova 2024)

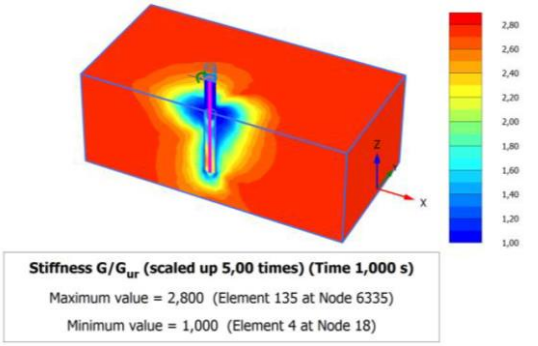

Figure 8. Soil stiffness G/G_{ur} around the monopile in the beginning of the cyclic loading in model 2 (HSsmall) (Rova 2024).

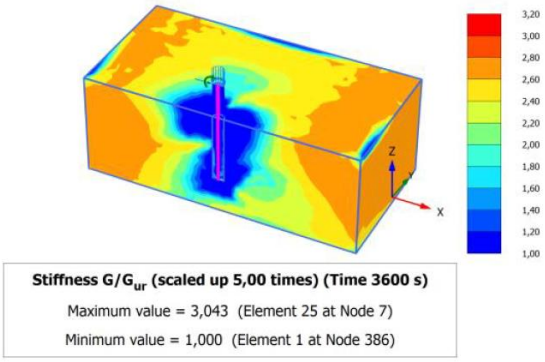

Figure 9. Soil stiffness G/G_{ur} around the monopile after the 1-hour cyclic loading in model 2 (HSsmall) (Rova 2024).

4 CONCLUSION

The use of the SANISAND-MS material model requires the user to pay particular attention to the soil parameters and other calculation software settings, such as mesh quality and appropriate size of the model geometry. The greatest influence on the operation of the SANISAND-MS was found to be the magnitude of the loads. During the modeling process, it was observed that the model failed to converge at high magnitude loads. Consequently, the modeling of a one-hour storm at maximum load was not possible. There is also possible that soil maximum resistance was reached under the dynamic analysis for which the maximum convergence was reached.

The use of the HSsmall material model did not present comparable difficulties during the modeling process as those encountered with the SANISAND-MS. The magnitude of the load had no impact on the convergence of the model. Nevertheless, the model does not accurately account for soil deformations in the dynamic analysis.

A comparison of the functionality of the material models was rendered difficult by the fact that SANISAND-MS was unable to model with maximum loads. It is therefore evident that HSsmall represents a simple way for simulating sandy soil in Plaxis 3D, particularly for large wind turbines with XL monopiles.

Furthermore, it is challenging to model cyclic loading and ascertain its duration. As illustrated in Model 5 (SANISAND-MS), the displacement increases even when a complete unloading situation occurs between each cyclic loading phase. In a static loading situation, it is not possible to analyze permanent displacements, which may result in an inaccurate estimation of the magnitude of the displacement.

Modeling simplifications have been made, for instance, in sandy soils where pore water is drained during the recovery phase of the cyclic load. However, neither of the material models used accounts for this phenomenon. A comprehensive material model for modeling sandy soils is expected in the future, which would simplify the calculation and modeling of the monopile foundation.

AUTHOR CONTRIBUTION STATEMENT

Milja Rova: Data curation, Formal Analysis, Writing- Original draft. **Anne Tuomela**.: Supervision, Writing- Reviewing and Editing. **Antti H. Niemi**: Supervision, Writing- Reviewing and Editing. **Janne Herva**: Supervision, Writing- Reviewing and Editing.

ACKNOWLEDGEMENTS

The financial support provided by Geobotnia Oy, Boskalis Oy, Rajakiiri Oy and Finnish Transport Infrastructure Agency is acknowledged.

5 REFERENCES

Arany, L., Bhattacharya, S., Macdonald, J. & Hogan, S. J., (2017). Design of monopiles for offshore wind turbines in 10 steps, Soil Dynamics and Earthquake Engineering, Vol 92, pp. 126–152, https://doi.org/10.1016/j.soildyn.2016.09.024, accessed 28/9/2024.

Bentley, (2023a). PLAXIS 3D 2023.2 SANISAND-MS UDSM. [online] Available at: [https://communities.bentley.com/], accessed 28/9/2024.

Bentley (2023b). PLAXIS 3D 2023.2 Reference Manual 3D. [online] Available at: [https://communities.bentley.com/], accessed 28/9/2024.

DNV-ST-0126 (2021). Support structures for wind turbines. Den Norske Veritas.

Gaertner, E., Rinker, J., Sethuraman, L., Zahle, F., Anderson, B., Barter, G., Abbas, N., Meng, F., Bortolotti, P., Skrzypinski, W., Scott, G., Feil, R., Bredmose, H., Dykes, K., Shields, M., Allen, C. & Viselli, A., (2020). Definition of the IEA Wind 15-Megawatt Offshore Reference Wind Turbine Technical Report, National Renewable Energy Laboratory, US.

Liu, H., Pisanò, F., Jostad, H. P. & Sivasithamparam, N., (2022). Impact of cyclic strain accumulation on the tilting behaviour of monopiles in sand: An assessment of the Miner's rule based on SANISAND-MS 3D FE modelling, Ocean Engineering, Vol 250 (110579), https://doi.org/10.1016/j.oceaneng.2022.110579, accessed 28/9/2024.

Liu, H., Diambra, A., Abell, J. A., & Pisanò, F., (2020). Memory-Enhanced Plasticity Modeling of Sand Behavior under Undrained Cyclic Loading, Journal of Geotechnical and Geoenvironmental Engineering, Volume 146 (11), pp. 1-14, https://doi.org/10.1061/(ASCE)GT.1943-5606.0002362, accessed: 28/9/2024.

Meng, X., Zhai, E. & Xu, C., (2024). A hypoplastic macroelement model for offshore wind turbine large-diameter monopiles in sand, Ocean Engineering, Vol 294 (116744), https://doi.org/10.1016/j.oceaneng.2024.116744, accessed 28/9/2024.

Ramírez, L., (2023). Wind Europe Market Intelligence. [online] Available at: windeurope.org, accessed 24/10/2023.

Rova, M., (2024). Geotechnical design of monopile foundation for offshore wind turbines (in Finnish). Master thesis, University of Oulu. Available at: https://oulurepo.oulu.fi/handle/10024/48802, accessed: 28/9/2024.

VTT, (2024). Ice-load portal, [online], Available at: [https://ice-load-portal.modellingfactory.com/], accessed 12/03/2024.

Wu, X., Hu, Y., Li, Y., Yang, J., Duan, L., Wang, T., Adcock, T., Jiang, Z., Gao, Z., Lin, Z., Borthwick, A. & Liao, S., (2019). Foundations of offshore wind turbines: A review, Renewable and Sustainable Energy Reviews, Vol 104, pp. 379–393, https://doi.org/10.1016/j.rser.2019.01.012, accessed 28/9/2024.